DOI: 10.1002/ange.201302894

Organic Nanophotonics

Controlling the Structures and Photonic Properties of Organic Nanomaterials by Molecular Design**

Wei Yao, Yongli Yan, Lin Xue, Chuang Zhang, Guoping Li, Qingdong Zheng, Yong Sheng Zhao, Hua Jiang,* and Jiannian Yao**

Controlling the flow of photons at the nano/microscale is crucial to the development of integrated optical circuits, which offer the potential to transmit and route information more efficiently than electronic circuits.[1] Because of the strong impact of the shape and dimensions of the photonic building blocks on the confinement and guiding of optical waves,[2] an essential strategy for controlling photonic flow is the fabrication of diverse structures. One-dimensional (1D) structures at the nano- and microscales, with field confinement in two dimensions, have been demonstrated as effective photonic elements, such as Fabry-Pérot (F-P) resonators,[3] waveguides,[4] lasers,[5] and transducers.[6] In comparison, two-dimensional (2D) sheet-like structures that confine photons in one dimension, can be integrated into a chip scale planar photonics system, including waveguides for interconnection, couplers, and modulators.[7]

Organic small molecules are attractive photonic materials because they exhibit high photoluminescence quantum efficiencies, color tunability, and size-dependent optical properties.[8] Moreover, flexibility in their synthesis and chemical modification makes organic molecules useful for the construction of various nanostructures.[9] Altering the organic molecular structure can tune the intermolecular interactions (π–π interaction, hydrogen bonding), which influence their packing mode during self-assembly and determine their final aggregated structures.[10] Self-assembly of aromatic organic molecules through strong π–π stacking is a common approach for forming 1D nanostructures with uniform morphological dimensions.[11] The introduction of a hydrogen-bonding group in specific positions would disturb the balance of π–π stacking, causing different preferential growth directions and nanostructures. Thus, the rational design of molecular components with different intermolecular recognitions would be promising for the construction of nanostructures with desired morphologies, which can confine and guide photons in specific dimensions.

Herein, we constructed 1D and 2D nanoarchitectures by altering the structures of the components of the self-assembled nanostructures, which is an important guide to the molecular design of tailor-made nanostructures and photonic properties. The molecules used in this study are naphthalene derivatives (Scheme 1) consisting of functional π systems. Introduction of different amino groups on the naphthalene core gave distinct intermolecular interactions that were favorable for 1D or 2D stacking arrangements. This geometrical discrepancy at the molecular level yields distinct nanostructures (1D nanowires and 2D rhombic nanosheets) with disparate photonic properties. The nanowires showed low transmission loss during the light propagation process, while the nanosheets displayed interesting asymmetric waveguiding behaviors, which we believe was determined by the molecular packing modes in the nanostructures. This method of controlling different structures and photonic properties by structural modification could provide insight and guidance for the development of organic-material-based photonic devices.

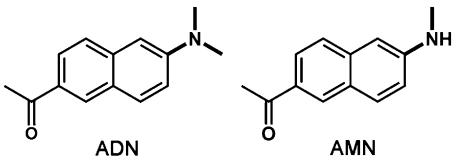

Scheme 1. Molecular formulas of the model compounds.

2-Acetyl-6-dimethylaminonaphthalene (ADN, Scheme 1) and 2-acetyl-6-methylaminonaphthalene (AMN) were synthesized (see Supporting Information) as model compounds,[12] to explore the influence of the substituents on their self-assembled nanostructures and photonic properties. Both molecules are semi-rigid and almost fully conjugated with the naphthalene core. Notably, ADN has a tertiary amine on the naphthalene core, while AMN has a secondary amine at the same position. This difference is expected to influence their intermolecular interactions and self-assembly behavior. AMN may have less steric repulsion with neighboring molecules compared with ADN when assembled into nanostructures. More importantly, the presence of an amide hydrogen-bonding site in AMN prevents packing along

[*] W. Yao, Dr. Y. Yan, Dr. L. Xue, C. Zhang, G. Li, Prof. Y. S. Zhao, Prof. H. Jiang, Prof. J. N. Yao
Beijing National Laboratory for Molecular Sciences (BNLMS), CAS Key Laboratory of Photochemistry, Institute of Chemistry, Chinese Academy of Sciences
Beijing 100190 (China)
E-mail: yszhao@iccas.ac.cn
hjiang@iccas.ac.cn
jnyao@iccas.ac.cn
Prof. Q. D. Zheng
State Key Laboratory of Structural Chemistry, Fujian Institute of Research on the Structure of Matter, Chinese Academy of Sciences (China)

[**] This work was supported by the National Natural Science Foundation of China (Nos. 21125315, 51203165), the Chinese Academy of Sciences, and the Ministry of Science and Technology of China (2012YQ120060 and National Basic Research 973 Program).
Supporting information for this article is available on the WWW under http://dx.doi.org/10.1002/anie.201302894.

a single direction, thus leading to nanostructures with different morphological features.

To determine the structural characteristics and intermolecular interactions of these compounds, we simulated the equilibrium shape of ADN and AMN crystals by minimizing the total surface energy using the Materials Studio package.[13] The crystal data and ORTEP drawing of the two single crystals used in the calculation are shown in the Supporting Information (Table S1 and Figure S1). From the simulation results, we found that the predicted growth pattern and thermodynamically stable morphology for compound ADN is a 1D wire-like structure (Figure 1 a). The calculated surface energies $\gamma(hkl)$ of the various crystal faces (hkl) follow the order: $\gamma(010) > \gamma(10\bar{2}) > \gamma(100) > \gamma(002)$ (Table S2). The (010) face, with the highest surface energy, is the preferred growth face because the kinetic barrier of growth for (hkl) is inversely proportional to the surface energy of $\gamma(hkl)$.[14] The ADN molecules are arranged in slip-stacks along the short molecular axis with a π–π stacking distance of 3.57 Å (Figure 1 b). Without H-bonding and other strong interactions between two adjacent molecules, the π–π interaction is the predominant driving force during self-assembly, which facilitates the ADN crystal growth along the [010] direction forming a 1D structure.

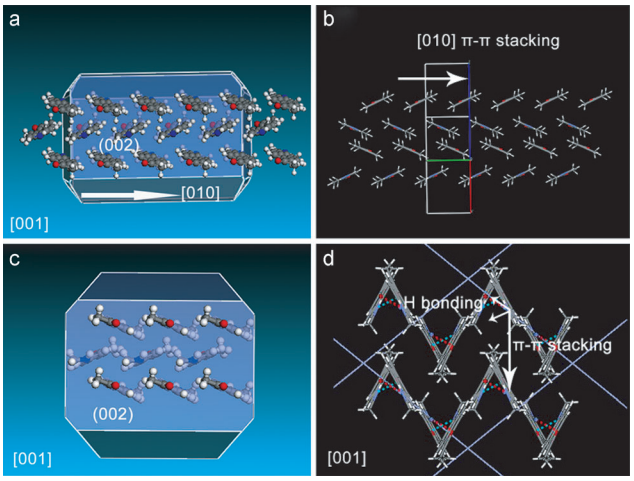

Figure 1. a) The predicted growth morphology of ADN molecules based on the attachment energies. b) The arrangement of ADN molecules under π–π stacking. c) The predicted growth morphology of AMN molecules based on the attachment energies. d) The packing arrangement of AMN molecules when viewed perpendicular to the (001) plane.

In contrast, simulation of the compound AMN using a growth morphology algorithm (Figure 1 c) gives a thermodynamically stable sheet-like structure. The larger attachment energies obtained from the (100) and (010) faces (Table S3) suggest that both the [100] and [010] directions have high growth rates. Figure 1 d shows the packing diagrams of AMN along the [001] crystal direction, where the four lavender lines indicate the (110) $(1\bar{1}0)$ $(\bar{1}10)$ $(\bar{1}\bar{1}0)$ planes. Besides π–π stacking along the *a* axis, there is also hydrogen bonding between the imide hydrogen and carbonyl oxygen with a separation of 2.96 Å. Hydrogen bonding advances the growth along the *b* axis, which results in a different packing behavior from that of the ADN molecules. Therefore, the intermolecular interactions of π–π stacking and hydrogen bonding cooperatively direct the self-assembly pathway toward the formation of 2D sheet-like structures by AMN.

The designed molecules were allowed to aggregate into their preferred morphologies by inducing self-assembly in the liquid phase. Depending on the intermolecular interactions, the molecules were expected to assemble into different nano- or sub-micrometer structures. The ADN molecules aggregated into 1D nanowires with a smooth surface and uniform diameter of about 800 nm (Figure 2 a). The TEM image and selected area electron diffraction (SAED) pattern in Figure 2 b reveal that the wires have single crystal structures growing along the [010] crystal direction. This direction can be attributed to the π–π interaction and is consistent with our calculated results. The nanowires exhibited intense blue emission under excitation of unfocused UV irradiation (330–380 nm) with the typical characteristics of an active optical waveguide, such as bright photoluminescent (PL) spots at the wire ends and weaker PL from the bodies (Figure 2 c). This indicates that PL energy can propagate efficiently along the axial direction, leading to a low-loss optical waveguide.

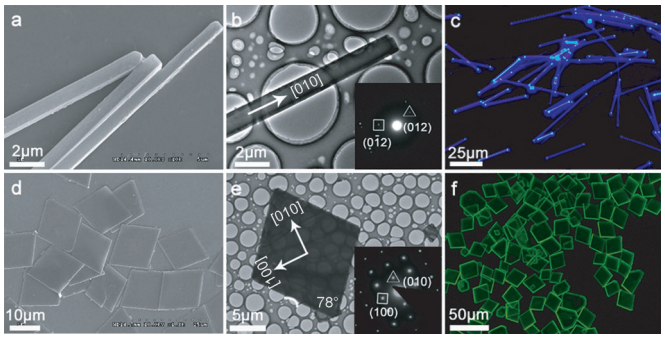

Figure 2. a) SEM and b) TEM images of the 1D nanowires aggregated from ADN molecules. Inset of (b): SAED pattern of a single wire. c) PL microscopy image of nanowires excited with the UV band of a mercury lamp. d) SEM and e) TEM images of the 2D rhombic nanosheets aggregated from AMN molecules. Inset of (e): SAED pattern of a single sheet. f) PL microscopy image of nanosheets excited with the UV band.

In contrast with ADN, AMN formed well-defined 2D rhombic nanosheets. These 2D nanosheets have an edge length of tens of micrometers (Figure 2 d, SEM image) and a thickness around 400 nm (Figure S2, AFM image). A typical TEM image of an individual nanosheet is given in Figure 2 e and its corresponding SAED patterns are shown in the inset. The SAED pattern can be indexed according to the crystal lattice constants of AMN (see Table S1). The SAED results indicate that the growth directions parallel to the substrate of the nanosheet are [100] and [010], which is determined by the π–π stacking and hydrogen-bonding interactions. As shown in the PL image in Figure 2 f, the bright green edges of the 2D

nanosheets indicate an obvious optical waveguiding characteristic and a strong 1D field confinement.

The optical waveguide properties of the as-prepared 1D nanowires and 2D nanosheets were studied to investigate the structure–property relationship of the nanostructures. Spatially resolved PL imaging and spectroscopy measurements were performed by locally exciting a single wire or sheet with a 351 nm focused laser beam. Figure 3a shows the micro-area

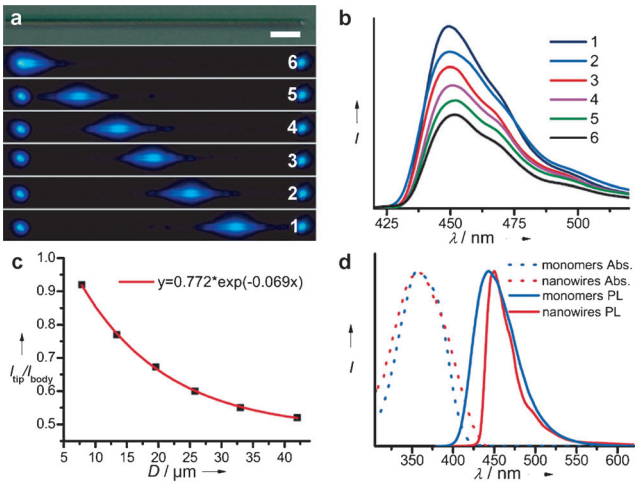

Figure 3. a) Bright-field and PL images obtained from a single ADN 1D nanowire by exciting the wire at different positions. Scale bar = 5 μm; b) Spatially resolved PL spectra from the tip of the nanowire for different separation distances between the excitation spot and tip of the wire shown in (a). c) The ratio of the intensity I_{tip}/I_{body} against the distance D. Curves were fitted by an exponential decay function $I_{tip}/I_{body} = A\exp(-RD)$. d) Normalized absorption and emission spectra of the ADN monomer and nanowires.

PL images obtained from a nanowire (length ≈ 40 μm) by accurately shifting the excitation laser spots. In this 1D structure, the photons are confined in two dimensions and propagate along the axis of the nanowires in two predominant transmission directions. The propagation loss of the materials was evaluated by looking at the spatially resolved spectra of the emitted light with respect to the distance travelled. Figure 3b illustrates the corresponding PL signals detected from the wire terminus by changing the position of the excitation laser beam.

The distance dependent intensity of the nanowire, shown in Figure 3c, indicates that the intensity of the out-coupled light decays almost exponentially with the increase in propagation distance, which is a typical characteristic of active waveguides. The intensity at the excited site along the body of the nanowire (I_{body}) and at the emitting tip (I_{tip}) were recorded and the optical-loss coefficient (R) was calculated by single-exponential fitting $I_{tip}/I_{body} = A\exp(-RD)$, where D is the distance between the excited site and the emitting tip.[15] Accordingly, $R = 0.069\ \mathrm{dB\,\mu m^{-1}}$ at 450 nm, which is much lower than the value for other organic materials.[16] There are two important factors that may contribute to the excellent optical waveguide behavior of the ADN nanowires. First, the smooth surface and high crystallinity minimized the optical loss caused by scattering. Second, the aggregation-induced red shift and narrowing of the fluorescent spectra reduced the overlap with its absorption spectra (Figure 3d), which can effectively diminish the reabsorption of light during propagation along the wire.

In contrast, the photons in the 2D nanosheets can migrate within the 2D plane parallel to the substrate with confinement in one dimension. One typical rhombic nanosheet with an edge length of about 30 μm (Figure 4a) was used to study the

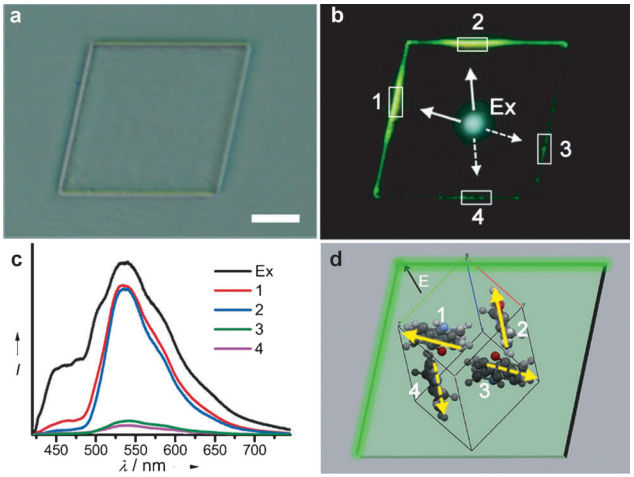

Figure 4. a) Bright-field and b) PL images obtained from a single AMN nanosheet by exciting the center with a UV laser ($\lambda = 351$ nm). Scale bar = 10 μm. Solid arrows show the predominant guiding directions; dashed arrows show the blocked directions. c) The corresponding spatially resolved PL spectra of the excited spot and the four edges (marked with 1–4) of the nanosheet shown in (b). d) The molecular packing arrangement in the sheet. Black arrow shows the direction of the electric field of incident light. Solid yellow arrows show the components of the transition dipole moments for the two front surface molecules (1, 2) in the (001) plane, while the dashed yellow arrows indicated those of the two molecules on the back side (3, 4).

light propagation behaviors in the 2D structure. As displayed in the photographs (Figure 4b), when the laser beam was focused at the center of the plane, the neighboring two out-coupled edges (marked with 1 and 2) have large, bright out-coupled light beams, which shows significant contrast with the small, obscure out-couplings at the opposite edges (3 and 4). This observation clearly indicates that the propagation efficiencies along the two opposite directions are entirely different. The corresponding PL spectra of the four edges (Figure 4c) quantitatively demonstrate that the emission intensities of edges 1 and 2 are hundreds of times stronger than that of their opposite edges, showing that the propagation efficiencies of these nanosheets are highly sensitive to the propagation direction. To estimate the asymmetry of the light propagation, we calculated the optical loss coefficient R in the different propagation directions according to the aforementioned formula. The loss coefficient R of the guide path towards edges 1 and 2 ($0.076\ \mathrm{dB\,\mu m^{-1}}$) is much lower than that for propagation along the opposite directions ($0.457\ \mathrm{dB\,\mu m^{-1}}$). It is this sharp difference in the loss behavior that results in the stark contrast in the output signals, which

confirms that these nanosheets could be applied for asymmetric light propagation in photonic circuits.

This asymmetric light propagation in the nanosheets is pertinent to the molecular-packing modes in the crystal, because the molecular stacking as well as the direction of its optical transition dipole determine the final optical properties.[17] If the electric field of the incident light is parallel to the transition dipole moment of oriented molecules, the PL is maximized with a high absorption cross section and propagation efficiency. In our case, the transition dipole of the AMN molecule is parallel to the naphthalene long axis in the π-conjugated plane, pointing in the direction of the amido groups. The well-defined rhombic nanosheet crystal has four AMN molecules in one unit cell, in which the four molecules display a centrosymmetric arrangement (Figure 4d; Figure S3). When a unit cell was excited, the emitted light was guided mainly along the directions of the components of the transition dipole for the two front molecules (solid arrows). As a result of this ensemble behavior, characteristic of repeated unit cells in a single-crystal nanosheet, the two out-coupled edges (Figure 4b, solid arrows) are much brighter than their opposite edges.

This asymmetric propagation makes the organic rhombic nanosheets suitable for optical planar diodes, which are optical analogues of the well-known and widely used electronic diodes.[18] By changing the input position on the nanosheet, we can achieve different functions for this optical device. When the excitation laser is focused on two opposite edges with the same excitation power, emitted light is allowed to travel from one side to the other in the forward direction, while transmission in the opposite direction is inhibited (Figure 5a,b). The corresponding PL spectra (Figure 5c) quantitatively demonstrated the excellent performance for unidirectional signal transfer with different loss coefficients R (0.106 dB μm^{-1} forward, and 0.573 dB μm^{-1} backward). The intensity contrast (C) between the two output edges is defined as $C=(I_1-I_2)/(I_1+I_2)$, where I_1 and I_2 are the forward and backward output intensity, respectively.[19] According to this formula, the calculated C value of the examined nanosheet is 0.89, which is high enough for applications in nanoscale photonic devices. By changing the size of the nanosheets (Figure S4), we can further control the propagation length to modulate the intensity contrast and diode efficiency. When the laser beam was focused on two opposite obtuse corners (Figure 5d,e), the nanosheet showed two asymmetric light propagation channels, providing a way to manipulate the photonic signals in multiple directions. According to the corresponding spatially resolved PL spectra (Figure 5f), the calculated C values of the two propagation channels are 0.93 and 0.88. We believe this kind of asymmetric propagation will play a fundamental role in creating a new generation of miniaturized all-optical logic devices.

In summary, we have controlled the formation of distinct self-assembled nanostructures (nanowires and nanosheets) and the photonic properties of organic materials by rational molecular design. Different dominant intermolecular interactions (H bonding, π–π stacking), based on molecular moieties with different structural and conformational characteristics, were responsible for the formation of organic nanostructures with distinct morphologies. The nanowires had low dissipation of light during propagation, while the nanosheets displayed interesting asymmetric light propagation, which originated from the molecular-packing modes in the aggregated nanostructure. The ability to asymmetrically propagate light makes these nanosheets promising candidates for optical planar diodes, which is important to control the flow of photons. These results should be useful for the investigation of active photonic devices and could have significant potential for future integrated photonic circuits.

Received: April 8, 2013
Published online: July 5, 2013

Keywords: materials science · nanophotonics · organic nanomaterials · self-assembly · waveguides

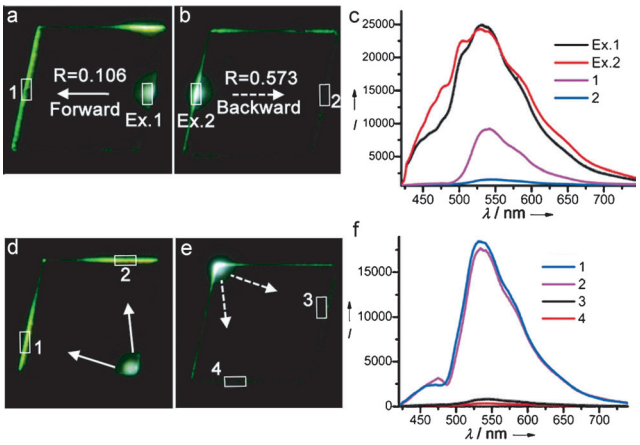

Figure 5. a,b) PL images obtained from a single sheet by exciting two opposite edges. c) The corresponding spatially resolved PL spectra of the excited spot and out-coupled edges (marked with 1,2) shown in (a,b). d,e) PL images obtained from the sheet by exciting two opposite obtuse corners. f) The corresponding spatially resolved PL spectra of the edges (marked with 1–4) shown in (d,e).

[1] a) D. J. Sirbuly, M. Law, P. Pauzauskie, H. Yan, A. V. Maslov, K. Knutsen, C. Z. Ning, R. J. Saykally, P. Yang, *Proc. Natl. Acad. Sci. USA* **2005**, *102*, 7800–7805; b) C. Zhang, Y. Yan, J. N. Yao, Y. S. Zhao, *Adv. Mater.* **2013**, *25*, 2854–2859.

[2] a) C. Zhang, Y. L. Yan, Y. Y. Jing, Q. Shi, Y. S. Zhao, J. N. Yao, *Adv. Mater.* **2012**, *24*, 1703–1708; b) N. Chandrasekhar, R. Chandrasekar, *Angew. Chem.* **2012**, *124*, 3616–3621; *Angew. Chem. Int. Ed.* **2012**, *51*, 3556–3561.

[3] a) X. F. Duan, Y. Huang, R. Agarwal, C. M. Lieber, *Nature* **2003**, *421*, 241–245; b) D. O'Carroll, I. Lieberwirth, G. Redmond, *Nat. Nanotechnol.* **2007**, *2*, 180–184.

[4] F. Balzer, V. Bordo, A. Simonsen, H. G. Rubahn, *Phys. Rev. B* **2003**, *67*, 115408.

[5] C. Zhang, C. L. Zou, Y. Yan, R. Hao, F. W. Sun, Z. F. Han, Y. S. Zhao, J. N. Yao, *J. Am. Chem. Soc.* **2011**, *133*, 7276–7279.

[6] J. Y. Zheng, Y. L. Yan, X. P. Wang, W. Shi, H. M. Ma, Y. S. Zhao, J. N. Yao, *Adv. Mater.* **2012**, *24*, OP194–OP199.

[7] a) L. Heng, X. Wang, D. Tian, J. Zhai, B. Tang, L. Jiang, *Adv. Mater.* **2010**, *22*, 4716–4720; b) H. Mizuno, U. Haku, Y. Marutani, A. Ishizumi, H. Yanagi, F. Sasaki, S. Hotta, *Adv. Mater.* **2012**, *24*, 5744–5749.

[8] a) Y. S. Zhao, H. B. Fu, F. Q. Hu, A. D. Peng, W. S. Yang, J. N. Yao, *Adv. Mater.* **2008**, *20*, 79 – 83; b) Y. S. Zhao, H. B. Fu, A. D. Peng, Y. Ma, D. B. Xiao, J. N. Yao, *Adv. Mater.* **2008**, *20*, 2859 – 2876.

[9] Y. Wang, J. Liu, H. D. Tran, M. Mecklenburg, X. N. Guan, A. Z. Stieg, B. C. Regan, D. C. Martin, R. B. Kaner, *J. Am. Chem. Soc.* **2012**, *134*, 9251 – 9262.

[10] a) Y. S. Zhao, H. B. Fu, A. D. Peng, Y. Ma, Q. Liao, J. N. Yao, *Acc. Chem. Res.* **2010**, *43*, 409 – 418; b) S. Yagai, Y. Goto, X. Lin, T. Karatsu, A. Kitamura, D. Kuzuhara, H. Yamada, Y. Kikkawa, A. Saeki, S. Seki, *Angew. Chem.* **2012**, *124*, 6747 – 6751; *Angew. Chem. Int. Ed.* **2012**, *51*, 6643 – 6647; c) Y. Yan, C. Zhang, J. N. Yao, Y. S. Zhao, *Adv. Mater.* **2013**, DOI: 10.1002/adma.201300325.

[11] T. Q. Nguyen, R. Martel, P. Avouris, M. L. Bushey, L. Brus, C. Nuckolls, *J. Am. Chem. Soc.* **2004**, *126*, 5234 – 5242.

[12] a) A. S. Rao, S. Singh, W. Choi, K. H. Ahn, *Org. Biomol. Chem.* **2012**, *10*, 8410 – 8417; b) A. Jacobson, A. Petric, D. Hogenkamp, A. Sinur, J. R. Barrio, *J. Am. Chem. Soc.* **1996**, *118*, 5572 – 5579.

[13] D. Winn, M. F. Doherty, *AIChE J.* **2000**, *46*, 1348 – 1367.

[14] J. W. Mullin, *Crystallization*, 3rd ed, Butterworth Heinemann, Oxford, **1992**, pp. 202 – 260.

[15] X. Wang, Y. Zhou, T. Lei, N. Hu, E.-Q. Chen, J. Pei, *Chem. Mater.* **2010**, *22*, 3735 – 3745.

[16] C. Zhang, Y. S. Zhao, J. N. Yao, *Phys. Chem. Chem. Phys.* **2011**, *13*, 9060 – 9073.

[17] a) D. O'Carroll, G. Redmond, *Chem. Mater.* **2008**, *20*, 6501 – 6508; b) Q. Bao, B. M. Goh, B. Yan, T. Yu, Z. Shen, K. P. Loh, *Adv. Mater.* **2010**, *22*, 3661 – 3666.

[18] H. Kurt, D. Yilmaz, A. E. Akosman, E. Ozbay, *Opt. Express* **2012**, *20*, 20635 – 20646.

[19] J. Y. Xu, X. J. Zhuang, P. F. Guo, W. Q. Huang, W. Hu, Q. L. Zhang, Q. Wan, X. L. Zhu, Z. Y. Yang, L. M. Tong, X. F. Duan, A. L. Pan, *Sci. Rep.* **2012**, *2*, 820.

